Optical Engineering

SPIEDigitalLibrary.org/oe

Suppressing low-order eigenmodes with local control for deformable mirrors

Rikard Heimsten
Mette Owner-Petersen
Thomas Ruppel
Douglas G. MacMynowski
Torben Andersen

Downloaded from SPIE Digital Library on 11 May 2012 to 131.215.220.186. Terms of Use: http://spiedl.org/terms

Optical Engineering 51(2), 026601 (February 2012)

Suppressing low-order eigenmodes with local control for deformable mirrors

Rikard Heimsten
Mette Owner-Petersen
Lund University
Lund Observatory
Box 43, SE-221 00 Lund
Sweden
E-mail: rikard.heimsten@telia.com

Thomas Ruppel
University of Stuttgart
Institute for System Dynamics
Postfach 80 11 40 D-70511 Stuttgart
Germany

Douglas G. MacMynowski
California Institute of Technology
Control and Dynamical Systems
1200 East California Boulevard
Pasadena, California 91125

Torben Andersen
Lund University
Lund Observatory
Box 43, SE-221 00 Lund
Sweden

Abstract. To improve the mechanical characteristics of actively controlled continuous faceplate deformable mirrors in adaptive optics, a strategy for reducing crosstalk between adjacent actuators and for suppressing low-order eigenmodes is proposed. The strategy can be seen as extending Saint-Venant's principle beyond the static case, for small local families of actuators. An analytic model is presented, from which we show the feasibility of the local control. Also, we demonstrate how eigenmodes and eigenfrequencies are affected by mirror parameters, such as thickness, diameter, Young's modulus, Poisson's ratio, and density. This analysis is used to evaluate the design strategy for a large deformable mirror, and how many actuators are needed within a family. © *2012 Society of Photo-Optical Instrumentation Engineers (SPIE).* [DOI: 10.1117/1.OE.51.2.026601]

Subject terms: distributed control; adaptive optics; large deformable mirror; dimensionless mode analysis.

Paper 110410 received Apr. 26, 2011; revised manuscript received Dec. 4, 2011; accepted for publication Dec. 7, 2011; published online Mar. 7, 2012.

1 Introduction

Most adaptive optics systems include a small deformable mirror, typically with a size of a few tens of millimeters, because it is much easier to achieve a high temporal bandwidth for a small mirror than for a large one. Integrating the deformable mirror into the telescope design, thus going from tens of millimeters to a few meters in diameter, will avoid lossy relay optics and make the telescope more compact.[1] Large deformable mirrors have successfully been integrated into the Multi Mirror Telescope[2] and the Large Binocular Telescope.[3]

Large deformable mirrors are generally implemented as thin shells of a glass ceramic with hundreds or thousands of actuators on the back. Often, there are also local deflection sensors on the back of the mirror for closed-loop control in combination with a wavefront sensor monitoring overall optical system quality.

Several types of actuators exist. Piezoelectric actuators are simple to control, but the strokes are small and the overall system cost becomes high due to tight manufacturing tolerances. Force actuators based upon the voice coil principle have the potential of large stroke and low cost, but are more difficult to control because the control system must handle the structural dynamics of the deformable mirror. We focus here on voice coil actuators.

0091-3286/2012/$25.00 © 2012 SPIE

Studies of multiple-input-multiple-output optimal controllers for deformable mirrors have shown good closed-loop performance.[4,5] However, neither the computational load nor the robustness of a global controller may be suitable for large deformable mirrors. In earlier publications,[6,7] we have studied a deformable mirror concept with faceplate, and low-cost force actuators and sensors, by numerical methods. This system has been demonstrated to work using a control system encompassing local control with position and velocity feedback. The local control concept was developed to suppress crosstalk between adjacent actuators as shown in Fig. 1. A command to a single actuator induces a tip/tilt to the whole mirror. If instead a local control scheme, encompassing a set of actuators, is used, the influence function of the controlled actuator can be made similar to a delta function. Hence, the local controllers only weakly excite low-order eigenmodes.

In this paper, we present an analytic model to study excitation of the various normal modes. An analysis is made to see how the control concept is affected by mirror dimensions. Further, we show how the eigenmodes and eigenfrequencies depend on mirror parameters. We validate our results by comparing the result obtained by the analytic model and a finite element model for a specific design.

2 Background

Design parameters of an actuator system for deformable mirrors involve optimal placement of the actuators and choice of control scheme. In practice, the actuator topology cannot be

Downloaded from SPIE Digital Library on 11 May 2012 to 131.215.220.186. Terms of Use: http://spiedl.org/terms

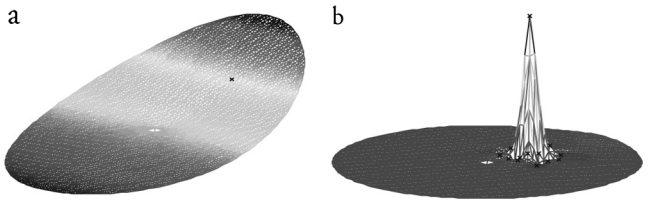

Fig. 1 An overview of the local control concept of the deformable mirror. (a) The influence function of a single actuator command. (b) The influence function of 21 actuator commands optimized to provide a local deflection.

chosen arbitrarily due to space constraints. We have assumed a Cartesian actuator topology, as shown in Fig. 2, and below we concentrate on selection and evaluation of a control strategy.

For the case in which the force actuators and the back position sensors are collocated and have a high bandwidth from DC to many kHz, it is possible to control each actuator independently with feedback from the collocated sensor only. By differentiating the position signal, a velocity signal can be obtained and an "electronic damper" can be implemented. Also, using the position signal, an "electronic spring" can be established at the location of an actuator and a sensor. Provided that the bandwidths of the actuator and sensor are sufficiently high, it can be readily seen that such a system can be made stable because no energy is injected into the system.[6] This solution has been used for medium-sized deformable mirrors.[8]

However, it is cumbersome from a design point of view to use collocated actuators and back sensors, and it is much less expensive to use position sensors placed between the actuators. These sensors can be implemented with electret microphones and bellows much like stethoscopes.[9] The challenge is that they do not provide a DC response; that is, they roll off with 20 dB/decade from about 20 Hz and downward to lower frequencies. Also, they do not work well at high frequencies due to resonances in the bellows.

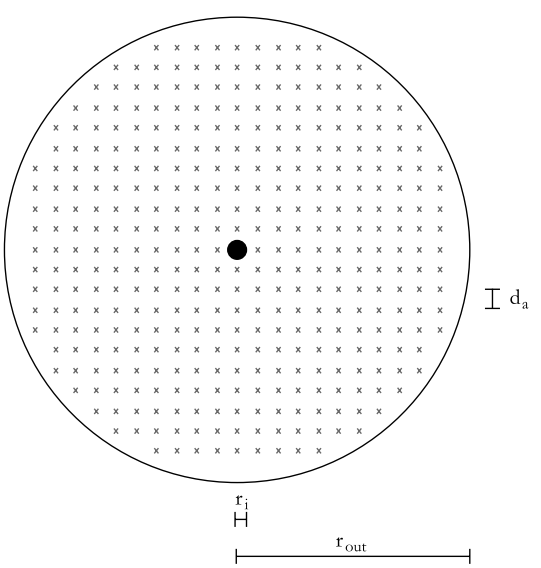

Fig. 2 An overview of the deformable mirror, which is clamped at the inner edge and free at the outer edge. The crosses illustrate the actuator topology. The actuator pitch d_a, inner hole radius r_i, and plate radius r_{out} are marked.

The same is true for the low-cost actuators referred to above. They are attached to the back of the mirror through suction cups having a certain compliance, leading to additional resonance effects. Although an internal loop in the actuator largely suppresses suction cup influence, the bandwidth of the actuators in practice is limited to some 2 to 3 kHz.

The task is therefore to develop a control system with a bandwidth of about 100 Hz for a thin mirror plate with bandwidth-limited actuators and sensors placed in a Cartesian topology. Introduction of a local control concept with "families" of actuators has proven advantageous because low-order eigenmodes are then only weakly excited.[7] An actuator family consists of a central actuator with one or more rings of actuators around it. Any actuator therefore belongs to more than one family. The force distribution in a given family is predetermined and scaled by an input signal to that family. Hence all forces in a family are in phase. In a previous paper,[6] we presented an approach for selection of a family force pattern, when a finite element model is available. Below, we give an analytical approach for determination of the pattern.

3 Mathematical Model

The deformable mirror plate is modeled as a solid, circular plate, with constant thickness h and an outer radius of r_{out} (see Fig. 2). It is centered at the origin of the $r-\phi$ plane, where r, ϕ are polar coordinates.

The time varying deflection of the mirror perpendicular to its surface with respect to the undeformed reference plate is called $w(r,\phi,t)$, where t is the time. The partial differential equation governing an undamped plate is given by[10]

$$D\nabla_r^4 w(r,\phi,t)+\rho h\frac{\partial^2 w(r,\phi,t)}{\partial t^2}=q(r,\phi,t), \tag{1}$$

where ρ is material density, D is the flexural rigidity, and $q(r,\phi,t)$ is the lateral load per unit area. The biharmonic operator ∇_r^4 is defined as

$$\nabla_r^4 \equiv \left(\frac{\partial^2}{\partial r^2}+\frac{1}{r}\frac{\partial}{\partial r}+\frac{1}{r^2}\frac{\partial^2}{\partial \phi^2}\right)^2.$$

The deformable mirror plate is clamped at its inner rim with a radius of r_i (see Fig. 2), which gives the boundary conditions

$$w(r_i,\phi,t)=0, \tag{2}$$

$$\left.\frac{\partial w}{\partial r}\right|_{r=r_i}=0, \tag{3}$$

since the lateral displacement and slope are zero. The outer edge is free, which gives the following boundary conditions:

$$D\left(\frac{\partial^2 w}{\partial r^2}+\frac{\nu}{r}\frac{\partial w}{\partial r}+\frac{\nu}{r^2}\frac{\partial^2 w}{\partial \phi^2}\right)\Bigg|_{r=r_{out}}=0, \tag{4}$$

Downloaded from SPIE Digital Library on 11 May 2012 to 131.215.220.186. Terms of Use: http://spiedl.org/terms

$$D\left[\frac{\partial}{\partial r}\nabla^4 w + (1-\nu)\frac{\partial^2}{\partial r^2}\left(\frac{1}{r^2}\frac{\partial w}{\partial r} - \frac{w}{r^3}\right)\right]\Bigg|_{r=r_{out}} = 0, \tag{5}$$

where the radial moment and radial shear forces are zero.[11] The term ν is Possion's ratio.

3.1 *Modal Analysis*

A parameterization by separation of variables as $w(r,\phi,t) = W(r,\phi)e^{-i\omega t}$ can be made,[12] where ω is the vibration frequency. Using the parameterization, the homogeneous version of Eq. (1) reads

$$\nabla_r^4 W(r,\phi) = \beta^4 W(r,\phi), \tag{6}$$

where $\beta^4 = \frac{\omega^2\rho h}{D}$. The general solution to Eq. (6) is given in Ref. 12 by

$$W(r,\phi) = W_{1,k}(r,\phi) + W_{2,k}(r,\phi), \tag{7}$$

$$\begin{aligned} W_{1,k}(r,\phi) &= [A_{1,k}J_k(\beta r) + A_{3,k}Y_k(\beta r)]\sin(k\phi) \\ &\quad + [A_{2,k}J_k(\beta r) + A_{4,k}Y_k(\beta r)]\cos(k\phi), \end{aligned} \tag{8}$$

$$\begin{aligned} W_{2,k}(r,\phi) &= [B_{1,k}I_k(\beta r) + B_{3,k}K_k(\beta r)]\sin(k\phi) \\ &\quad + [B_{2,k}I_k(\beta r) + B_{4,k}K_k(\beta r)]\cos(k\phi), \end{aligned} \tag{9}$$

where J_k and Y_k are Bessel functions of order $k \in \mathbb{N}$ and of the first and second kind, respectively. The second term of Eq. (7) involves the modified Bessel functions I_k and K_k of the order k and of the first and second kind. Thereby, the following equivalent relations hold[13]

$$I_k(x) = i^{-k}J_k(ix)$$

$$\begin{aligned} Y_k(x) = \frac{1}{\pi}\Bigg\{2\left(\gamma + \ln\frac{x}{2}\right)J_k(x) - \sum_{n=0}^{k-1}\frac{(k-n-1)!x^{2n-k}}{2^{2n-k}n!} \\ - \sum_{n=0}^{\infty}\frac{(-1)^n\chi[k+n+\chi(n)]x^{k+2n)}}{2^{k+2n}n!(k+n)!}\Bigg\}, \end{aligned}$$

with

$$\chi(n) = \begin{cases} 0 & \text{if } n = 0 \\ \sum_{l=1}^{n}\frac{1}{l} & \text{if } n > 0 \end{cases}$$

$$K_k(x) = \frac{\pi}{2}i^{k+1}[J_k(ix) + iY_k(ix)],$$

with $i = \sqrt{-1}$ and γ being the Euler constant.

3.2 *Participation Factor*

The modal participation factor measures the coupling between an exciting point force and a given mode shape. An analytic expression for the modal participation factor will now be determined.

The deflection of the mirror can be written using a superposition of the eigenmodes as

$$w(r,\phi,t) = \sum_{k=1}^{\infty} c_k W_k(r,\phi)e^{-i\omega t}, \tag{10}$$

where $W_k(r,\phi)$ is the kth eigenmode and c_k the participation factor, with the dimension of length, of that normal mode. We define $W_k(r,\phi)$ as the dimensionless eigenmode satisfying the orthonormality relations

$$\frac{1}{A}\int_{r_i}^{r_{\text{out}}}\int_0^{2\pi} W_k(r,\phi)W_l(r,\phi)r\mathrm{d}r\mathrm{d}\phi = \delta_{k,l},$$

where $\delta_{k,l}$ is the Kronecker delta and A is the total area of the plate. The external load reads

$$q(r,\phi,t) = u\frac{1}{r}\delta(r-R)\delta(\phi-\Phi)e^{-i\omega t} \tag{11}$$

for a point force u at the position (R,Φ) where $\delta(x)$ is Dirac's delta function, which then gives[14]

$$\int_0^{\infty}\int_0^{2\pi}\frac{1}{r}\delta(r-r')\delta(\phi-\phi')r\mathrm{d}\phi\mathrm{d}r = 1.$$

Using Eq. (10) to describe the deflection of the plate and Eq. (11) to describe the external forces, use of the plate dynamics Eq. (1) gives

$$\begin{aligned} &D\nabla_r^4\sum_{k=1}^{\infty}c_kW_k(r,\phi) - \rho h\omega^2\sum_{k=1}^{\infty}c_kW_k(r,\phi) \\ &\quad = u\frac{1}{r}\delta(r-R)\delta(\phi-\Phi), \end{aligned}$$

where $e^{-i\omega t}$ has been eliminated from the equation. Using the identity of the eigenfunctions, given by Eq. (6), this equation can be simplified to

$$\rho h\sum_{k=1}^{\infty}(\omega_k^2-\omega^2)c_kW_k(r,\phi) = u\frac{1}{r}\delta(r-R)\delta(\phi-\Phi). \tag{12}$$

Multiplying with one specific eigenmode $W_l(r,\phi)$ and integrating over the full plate gives

$$\begin{aligned} &\int_{r_i}^{r_{\text{out}}}\int_0^{2\pi}W_l(r,\phi)\rho h\sum_{k=1}^{\infty}(\omega_k^2-\omega^2)c_kW_k(r,\phi)r\mathrm{d}r\mathrm{d}\phi \\ &\quad = \int_{r_i}^{r_{\text{out}}}\int_0^{2\pi}W_l(r,\phi)u\frac{1}{r}\delta(r-R)\delta(\phi-\Phi)r\mathrm{d}r\mathrm{d}\phi. \end{aligned}$$

The left-hand side can be reduced by using the orthonormality condition of the eigenmodes, and the right-hand side is reduced, since the Dirac delta function is zero outside (R,Φ). Thus, the participation factor can be expressed as

$$A\rho h(\omega_l^2-\omega^2)c_l = uW_l(R,\Phi) \quad c_l = \frac{uW_l(R,\Phi)}{M(\omega_l^2-\omega^2)},$$

where M is the total mass of the plate. The unrealistic behavior of $c_l \to \infty$ when $\omega \to \pm\omega_l$ occurs because the damping of the system has yet not been considered.

Downloaded from SPIE Digital Library on 11 May 2012 to 131.215.220.186. Terms of Use: http://spiedl.org/terms

Table 1 Parameter values for a 1-m deformable mirror used for performance studies.

Parameter	Definition	Value
E	Young's modulus	63×10^9 Pa
ρ	density	2.23×10^3 kg/m^3
ν	Poisson ratio	0.2
h	thickness	2 mm
D	bending stiffness	$Eh^3/12(1-\nu^2)$
r_{out}	radius of the mirror	0.5 m
r_i	radius of the inner hole	0.025 m
d_a	actuator pitch	0.045 m
ζ	damping ratio	1%

4 Results

In Sec. 4.1, a dimensionless mode analysis is made for the mirror layout in Fig. 2. The example case used to derive the results presented in Secs. 4.2 to 4.4 is a mirror made of borosilicate. The parameters are given in Table 1.

4.1 *Dimensionless Mode Analysis*

We perform a dimensionless modal analysis to establish the relationship between the normal modes and design parameters, such as thickness, Poisson's ratio, bending stiffness, and mirror dimensions. The analysis is valid for any given plate with the same r_{out}/r_i ratio as shown in Fig. 2. The dimensionless quantity ξ is defined as

$$\xi = \frac{r}{r_{out}}.$$

The biharmonic operator, ∇^4_ξ, for the coordinate plane $\xi - \phi$ is related to ∇^4_r as

$$\nabla^4_r = \left(\frac{1}{r_{out}}\right)^4 \nabla^4_\xi.$$

Thus, the homogenous equation given in Eq. (6) is changed to

$$\mathrm{rcl}\nabla^4_\xi W(\xi,\phi) = \alpha^4 W(\xi,\phi),$$

where $\alpha^4 = \frac{r^4_{out}\omega^2\rho h}{D}$. To determine the eight coefficients of Eq. (7), the boundary conditions of the plate are used. The coefficients can be computed considering the sine and cosine parts of Eq. (7) independently.[15] Thus, two sets of four equations can be used to determine the corresponding coefficients $(A_{1,k}, A_{3,k}, B_{1,k}, B_{3,k})$ and $(A_{2,k}, A_{4,k}, B_{2,k}, B_{4,k})$. The resulting equations can be written in matrix form as

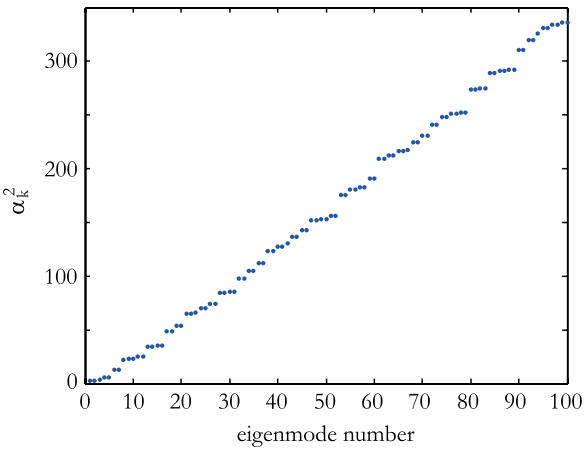

Fig. 3 The first hundred α_k^2 values for a mirror with the layout of Fig. 2, where $r_{out}/r_i = 20$.

$$\Lambda(\alpha_k)_{\sin}\begin{Bmatrix} A_{1,k} \\ A_{3,k} \\ B_{1,k} \\ B_{3,k} \end{Bmatrix} = 0 \qquad \Lambda(\alpha_k)_{\cos}\begin{Bmatrix} A_{2,k} \\ A_{4,k} \\ B_{2,k} \\ B_{4,k} \end{Bmatrix} = 0, \tag{13}$$

where $\Lambda(\alpha_k)_{\sin}$ and $\Lambda(\alpha_k)_{\cos}$ are 4-by-4 matrices with elements determined by the boundary conditions. The equivalent boundary conditions in Eqs. (2) and (4) for $w(\xi,\phi,t)$ depend only on the physical parameter ν. Thus, the normal modes depend on Poisson's ratio, the r_{out}/r_i ratio, and the α_k's. The eigenfrequencies for the eigenmodes are found by

$$\det[\Lambda(\alpha_k)] = 0,$$

which must hold for all nontrivial solutions of Eq. (13). The values of α_k are dimensionless and they are the same for any given mirror with the same r_{out}/r_i ratio and the same Poisson's ratio. The eigenfrequencies, ω_k, are given by

$$\frac{\omega_k}{\omega_0} = \alpha_k^2 \quad \text{for } \omega_0 = \sqrt{\left(\frac{1}{r_{out}}\right)^4 \frac{Eh^2}{12\rho(1-\nu^2)}}, \tag{14}$$

where ω_0 is unique for the mirror. Note that as $r_{out} \to \infty$, all eigenfrequencies go to zero. Thus, only a plate of finite size will have eigenmodes, formed by reflection of bending waves by the boundaries. Also the ratio between two specific eigenfrequencies will remain the same regardless of the specific value of ω_0. The first hundred α_k values for a mirror with a a ratio of 20 between the outer and inner radius are shown in Fig. 3. When ω_0 and the α_k's are given, the number of normal modes that must be controlled within a given bandwidth will also be given. The example case in Table 1 gives a value of ω_0 equal to 12.53 rad/s. Thus, there are eighteen normal modes within the bandwidth of the adaptive optics system (i.e., below 100 Hz) and five normal modes below the cutoff frequency (20 Hz) for the back sensors.

4.2 *Force Patterns Analysis*

The influence function for one actuator resembles a tip/tilt mode, because this mode is most compliant (see Fig. 1). Thus, the actuator families should be designed to suppress

Downloaded from SPIE Digital Library on 11 May 2012 to 131.215.220.186. Terms of Use: http://spiedl.org/terms

the low-order eigenmodes to reduce crosstalk between adjacent actuators. We now derive an analytic expression to determine the optimal force patterns for a given actuator family. A cost function is formed for the deviation between the static deflection of the mirror and the desired deflection. The force patterns are found by minimizing the cost function, using a least-squares approach.

An actuator family has a "master" actuator (most often located in the center of the family) at which the desired deflection is one. Elsewhere on the mirror, the deflection should be close to zero. The desired deflection for the mirror then is

$$\frac{1}{r}\delta(r-R_j)\delta(\phi-\Phi_j), \tag{15}$$

when the j'th actuator is controlled (i.e. the desired influence function for a family is a Dirac function). The deflection of the mirror is given through superposition of the individual normal modes as defined by Eq. (10), and the participation factors are given by Eq. (13). For the static case, ω is equal to zero; thus, for a single force u at (R, Φ), the deflection invoking m normal modes is

$$w(r,\phi)=\frac{1}{M}\sum_{k=1}^{m}\frac{W_k(r,\phi)}{\omega_k^2}uW_k(R,\Phi).$$

When multiple forces u_i are applied to the plate at different locations (R_i,Φ_i), the equation becomes

$$w(r,\phi)=\frac{1}{M}\sum_{k=1}^{m}\left[\frac{W_k(r,\phi)}{\omega_k^2}\sum_{i=1}^{n}u_iW_k(R_i,\Phi_i)\right]. \tag{16}$$

The squared error over the whole mirror, i.e. the cost function, is

$$J=\int_0^{2\pi}\int_{r_i}^{r_{\text{out}}}f(r,\phi,u_i)^2r\mathrm{d}r\mathrm{d}\phi,$$

where

$$f(r,\phi,u_i)=\frac{1}{M}\sum_{k=1}^{m}\left[\frac{W_k(r,\phi)}{\omega_k^2}\sum_{i=1}^{n}u_iW_k(R_i,\Phi_i)\right]-\frac{1}{r}\delta(r-R_j)\delta(\phi-\Phi_j).$$

Minimizing J with respect to u_l gives

$$\frac{\partial J}{\partial u_l}=\int_0^{2\pi}\int_{r_i}^{r_{\text{out}}}2f(r,\phi,u_i)\frac{\partial f(r,\phi,u_i)}{\partial u_l}r\mathrm{d}r\mathrm{d}\phi=0.$$

The above equation results in

$$\sum_{k=1}^{m}\left[\frac{W_k(R_l,\Phi_l)}{\omega_k^4}\sum_{i=1}^{n}u_iW_k(R_i,\Phi_i)\right]=M\sum_{k=1}^{m}\frac{W_k(R_l,\Phi_l)}{\omega_k^2}W_k(R_j,\Phi_j).$$

The equation system to determine the force u_i can be written in matrix form as

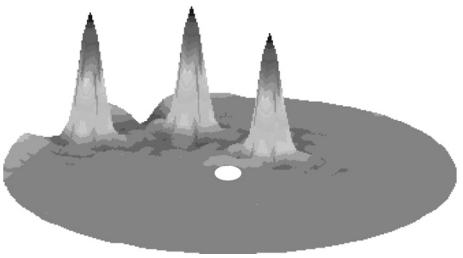

Fig. 4 The plate deflection of the mirror is shown for three different actuator family commands, when using 21 actuators in a family.

$$\mathbf{Au}=\mathbf{b}, \tag{17}$$

where the elements in the matrix $\mathbf{A}$ and the vector $\mathbf{b}$ are given by

$$a_{il}=\sum_{k=1}^{m}\frac{W_k(R_l,\Phi_l)}{\omega_k^4}W_k(R_i,\Phi_i)$$

$$b_l=M\sum_{k=1}^{m}\frac{W_k(R_l,\Phi_l)}{\omega_k^2}W_k(R_j,\Phi_j).$$

To summarize the notations, we note that k is the number of the normal mode, m the number of normal modes considered, i the column number of the matrix $\mathbf{A}$, l the row number of the matrix $\mathbf{A}$ and the vector $\mathbf{b}$, and j the actuator being controlled. $\mathbf{A}$ is a square matrix, since both i and l are running from 1 to the number n of actuators in the family. The solution for $\mathbf{u}$ includes the modal stiffness $M\omega_k^2$ and describes the relative distribution of forces within a family with a given location. The corresponding deflection is found from Eq. (16).

For our example, we have studied a family with a center actuator and two rings of actuators around it. Finding the force pattern as described above, we have determined the mirror deflection shown in Fig. 4 for a unity command to each of three families located at different places on the mirror. The influence functions of the families are almost identical over the mirror. At the outer edge, a waffle pattern exists around the family. However, the total root mean square value of the differences between the mirror deflection and the commanded shape over the mirror remains small.

In order to compute the force commands within a given family with sufficient accuracy, it is important to consider a large number of normal modes. This is illustrated in Fig. 5, showing the deflection of the mirror for three cases using the same force excitation. A different number of normal modes, m, have been included, when computing the deflection. The correct force pattern can only be found if the eigenmodes can reproduce the desired influence function within sufficient accuracy. This also implies that the number of normal modes needed depends on the relative actuator pitch, i.e. the total number of actuators. For a given actuator pitch, there is a maximum number of normal modes that can be controlled, and this will also roughly be the number of normal modes needed to determine the correct force pattern.

Downloaded from SPIE Digital Library on 11 May 2012 to 131.215.220.186. Terms of Use: http://spiedl.org/terms

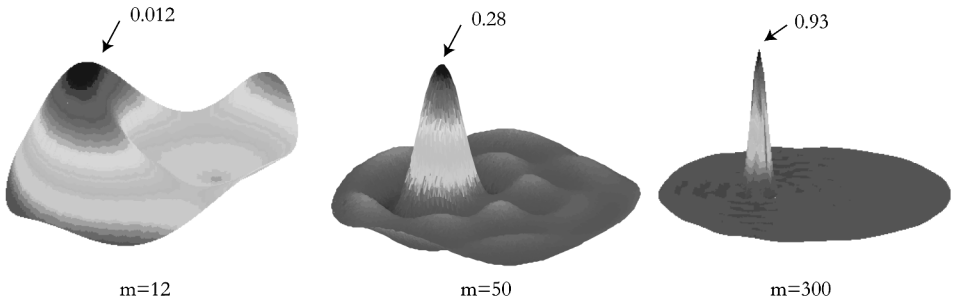

Fig. 5 Mirror deflection for the plate example. The same family force input was applied in all three cases but a different number of modes, *m*, was used in computing the responses.

4.3 *Frequency Response Analysis*

We now derive expressions for frequency responses from forces to mirror deflection. Referring to Eq. (13), the participation factor is

$$c_l = \frac{uW_l(R,\Phi)}{M(\omega_l^2 - \omega^2)} \,. \tag{18}$$

The transfer function from a force to displacement at the same location is determined by inserting Eq. (18) into Eq. (10), which gives

$$\frac{w(R,\Phi)}{u} = \sum_{k=1}^{m} W_k(r,\phi)W_k(R,\Phi)\frac{1}{M(\omega_k^2 - \omega^2)}. \tag{19}$$

Due to lack of damping in our model, the term $(\omega_k^2 - \omega^2)$ converges toward zero for $\omega \to \omega_k$. To include the effect of damping, we take analogy in the frequency response of a conventional second-order system

$$\frac{x(\omega)}{f(\omega)} = \frac{1}{M_o(\omega_k^2 - \omega^2 + 2i\zeta_k\omega_k\omega)},$$

where M_o is the generalized mass, ζ_k the damping ratio, x the displacement, and f the force. By analogy, we can therefore as an approximation introduce damping in Eq. (19) by replacing $(\omega_k^2 - \omega^2)$ with $(\omega_k^2 - \omega^2 + 2i\zeta_k\omega_k\omega)$, whereby we get

$$c_l = \frac{uW_l(R,\Phi)}{M(\omega_l^2 - \omega^2 + 2i\zeta_l\omega\omega_l)}, \tag{20}$$

which now encompasses an imaginary term. Inserting Eq. (20) into Eq. (10) and considering that multiple force are applied, the transfer function from force to position reads

$$\frac{w(R,\Phi)}{u} = \sum_{k=1}^{m}\left[\frac{W_k(R,\Phi)}{M(\omega_k^2 - \omega^2 + 2i\zeta_k\omega\omega_k)}\sum_{i=1}^{n} u_i W_k(R_i,\Phi_i)\right]. \tag{21}$$

The transfer function is evaluated at the point (R,Φ) where the force u is applied, and u_i is the relative magnitude between the force applied at the location (R_i,Φ_i) and u. For our example, four frequency responses for a representative actuator location are shown in Fig. 6. The curves are the transfer functions determined from Eq. (21) (for $m = 35$), where the output is the plate deflection at the center of

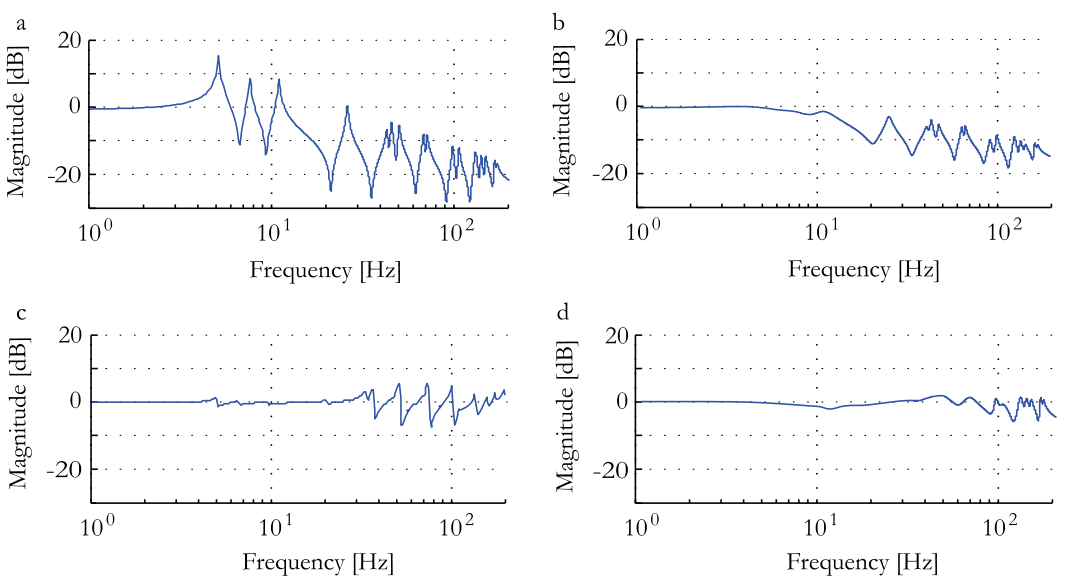

Fig. 6 The frequency response for a representative actuator located 0.25 m from the center, from force to position for: (a) the plate, (b) the plate with families of 9 actuators, (c) the plate with families of 21 actuators, and (d) the plate with families of 59 actuators. The frequency responses are determined with 35 eigenmodes.

Downloaded from SPIE Digital Library on 11 May 2012 to 131.215.220.186. Terms of Use: http://spiedl.org/terms

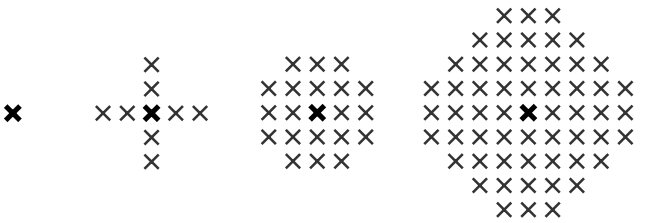

Fig. 7 The four family patterns used to evaluate the participation factor.

the family and the input is the force command for the single actuator case and for three different family patterns. Using a family, the resonance and antiresonance peaks are attenuated up to a frequency dependent on the number of actuators in the family. If a control system needs a flat frequency response up to a certain frequency, the number of actuators in the family should be chosen accordingly.

4.4 *Local Control Analysis*

Three patterns of the local family, including 9, 21, and 59 actuators, are evaluated against the single-input-single-output case, as shown in Fig. 7. A modified version of Eq. (13) is used to compute the participation factor, which then is, neglecting damping,

$$c_{l,n} = \frac{1}{M(\omega_l^2 - \omega^2)} \sum_{i=1}^{n} u_i W_l(R_i, \Phi_i),$$

where n is the number of actuators in the family, and u_i the force computed from Eq. (17). The evaluation of the family concept is done by computing the modal quality factors

$$\mathcal{Q}_9 = \frac{c_{l,9}}{c_{l,1}} \quad \mathcal{Q}_{21} = \frac{c_{l,21}}{c_{l,1}} \quad \mathcal{Q}_{59} = \frac{c_{l,51}}{c_{l,1}}.$$

These quality factors are independent of ω, ω_l, and M, and are valid for any plate with the same number of actuators and the same topology. They define the mode-suppression a given family can provide.

For the first twenty normal modes, we present in Fig. 8 the quality factor averages $\bar{\mathcal{Q}}$ for all families on a logarithmic scale. The families encompassing more actuators have more degrees of freedom, which means they should be able to attenuate more eigenmodes. This effect is seen in Fig. 8, where the performance differences between the families increase with the order of the normal mode. The improvement of the quality factor for the eighth, 15th, and 20th eigenmodes has the same origin. These three eigenmodes have rotational symmetry, which gives low curvature and low modal stiffness in the radial direction within the families. Because it is sufficient to block excitation in either radial or azimuthal direction, these eigenmodes stand out in Fig. 8.

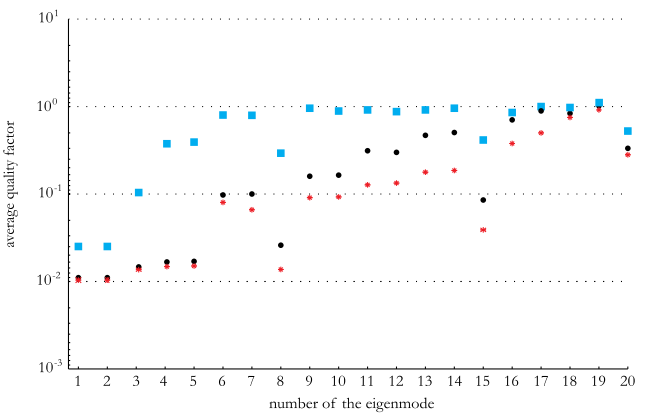

Fig. 8 The plot shows the average quality factors $\bar{\mathcal{Q}}_{59}$, $\bar{\mathcal{Q}}_{21}$, and $\bar{\mathcal{Q}}_9$ for the first 20 eigenmodes. The squares are for $\bar{\mathcal{Q}}_9$, the circles are for $\bar{\mathcal{Q}}_{21}$, and the stars are for $\bar{\mathcal{Q}}_{59}$.

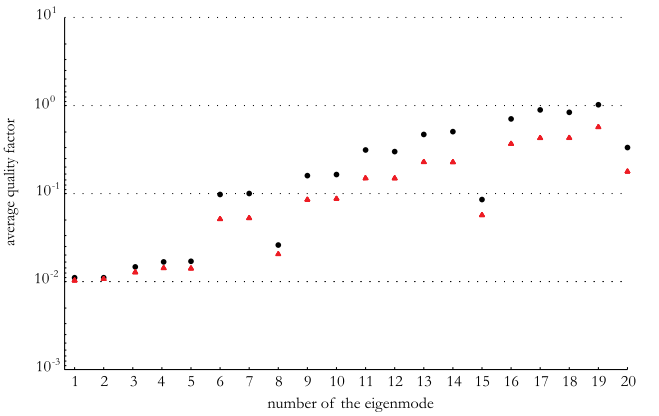

Fig. 9 The plot shows the average quality factor $\bar{\mathcal{Q}}_{21}$ for the 20 first eigenmodes. The circles correspond to a relative actuator pitch of 0.09 and the triangles are correspond to relative actuator pitch of 0.045.

The number of eigenmodes attenuated are close to half the number of degrees of freedoms in the families. This statement is only partially true for 59 actuators, because the area that the family occupies also increases. This effect is

Table 2 A comparison of the twelve first eigenfrequencies as determined by the analytical and the finite element model. Note that ω_0 here is equal to 12.53 Hz.

	Analytic model	Finite element model	Deviation
ω_1	32.7 rad/s	35.2 rad/s	2.5 rad/s
ω_2	32.7 rad/s	35.2 rad/s	2.5 rad/s
ω_3	48.4 rad/s	48.4 rad/s	0 rad/s
ω_4	69.7 rad/s	70.2 rad/s	0.5 rad/s
ω_5	69.7 rad/s	70.2 rad/s	0.5 rad/s
ω_6	164.6 rad/s	163.3 rad/s	1.3 rad/s
ω_7	164.6 rad/s	163.3 rad/s	1.3 rad/s
ω_8	280.4 rad/s	280.1 rad/s	0.3 rad/s
ω_9	286.1 rad/s	284.7 rad/s	1.4 rad/s
ω_{10}	287.1 rad/s	284.7 rad/s	2.4 rad/s
ω_{11}	312.1 rad/s	310.1 rad/s	2.0 rad/s
ω_{12}	312.1 rad/s	310.1 rad/s	2.0 rad/s

Downloaded from SPIE Digital Library on 11 May 2012 to 131.215.220.186. Terms of Use: http://spiedl.org/terms

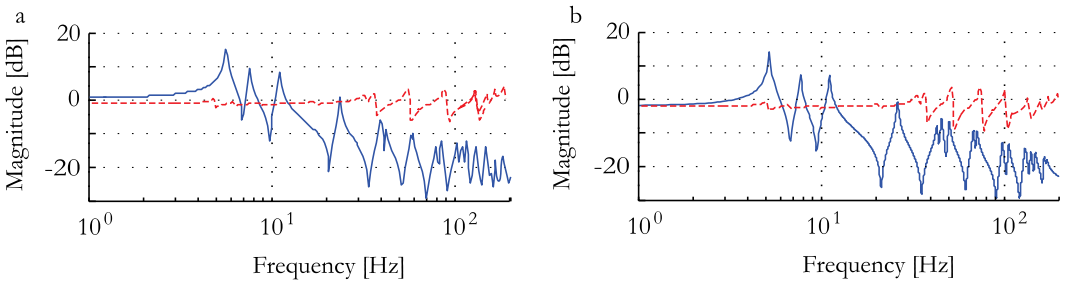

Fig. 10 Frequency responses from force to position for an actuator placed 0.25 m from the center. The full curve is the response for which the input is the force at one actuator and the output is the mirror deflection at the same location. The dashed line is the frequency response, where the input is the force command to a family of 21 actuators and the output is mirror deflection at the center actuator. The curves of (a) are determined with the finite element model (b) with the analytical model including 35 normal modes.

shown in Fig. 9, where the average quality factor is evaluated against the mode number with the relative actuator pitch d_a/r_{out} as parameter. Thus, doubling the mirror diameter or halving the actuator pitch has the same effect on the quality factors. Conclusively, more actuators on a given plate suppress more eigenmodes for a given number of actuators in the family, or a family with the same actuator pitch and the same number of actuators will suppress more eigenmodes on a 3-m mirror than on a 1-m mirror.

4.5 *Comparison Between the Analytical and the Finite Element Model*

We have performed a comparison between the results of the analytical model presented above and a finite element model.[6] The forms of the eigenmodes agree well with those of the finite element model. The differences in the corresponding eigenfrequencies are shown in Table 2. The deviation between the values from the two models is rather small, about 5%.

For the same example, the frequency responses from force to position of the two models for the same representative actuator location are seen in Fig. 10. The full lines represent the single actuator case, where the input is the force of a single actuator and the output is the mirror deflection at the same location. The dashed line is a frequency response for which the input is the command to an actuator family of 21 actuators and the output is the mirror deflection at the location of the center actuator of the family. There is good agreement between the plots of the analytical and finite element models. The minor shifts in the location of the resonance and anti-resonance peaks are due to the eigenfrequency deviation.

For our example, the family force patterns found using the expressions of Sec. 4.2 match well with those derived using the finite element model.[6] The two force patterns agree within 5%, and the deviation decreases with an increased number of modes considered in Eq. (17).

5 Conclusion

We have set up an analytical model of a deformable mirror and derived expressions for local control using families of actuators. Eq. (17), based on the least-squares method, can be used to optimize the influence function of a master actuator. The influence function will be similar for any size and type of mirror; that is, the size of the peak only depends on the relative actuator pitch and the number of actuators in the family. The concept ensures that the actuators only excite low-order modes of the plate weakly, which is particulary important, when using back sensors based upon low-cost electret microphones. The sum of the forces and moments for one family is close to zero, so the concept can be seen as an extension of Saint-Venant's principle to the dynamical case.

The analytical model can be applied for system design without use of a finite element model. In particular, the model is useful for studies of the influence of parameter variations and for determination of usable parameter space. We have shown how the parameters of mirrors with the same ratio between the outer and inner edge affect the eigenmodes and eigenfrequencies. Mirrors with the same Poisson's ratio will have the same relative eigenmodes for the same boundary conditions. We have introduced a parameter α_k, which is the same for all such mirrors. The use of α_k makes it possible to predict how eigenfrequencies are influenced by changes of physical parameters. For instance, the effects of doubling the diameter of a deformable mirror are:

1. Equation (14) shows that ω_0 scales with $1/r_{\text{out}}^2$ and Fig. 3 shows that the α_k's are close to linearly distributed for the first hundred normal modes. Thus, doubling r_{out} will roughly quadruple the number of of normal modes within a given bandwidth.
2. The relative actuator pitch d_a/r_{out} will be halved if the actuator pitch is kept the same. For a given family pattern, this will improve the quality factors (see Fig. 9).

The first effect is the dominant one, thus resulting in a more difficult system to control when increasing the diameter of the deformable mirror. The remedy, if needed, is either to increase the number of actuators within the families or to change the other physical parameters to counteract the effect from doubling r_{out}, according to Eq. (14).

For specific types of actuator families and using an example, we have compared results from the analytical model with those from a finite element model and found good agreement, both for eigenfrequencies, eigenmodes, frequency responses, and family force patterns. The combined modal participation factor for an actuator family can be up to 60 times lower than the modal participation factor for a single actuator in our example. The effect is also seen in the frequency response from force to position for our example, where resonance peaks below 40 Hz have been attenuated even with a conservative 1% modal damping used in our

Downloaded from SPIE Digital Library on 11 May 2012 to 131.215.220.186. Terms of Use: http://spiedl.org/terms

model. This is well above the cutoff frequency for the back sensors.

References

1. J. Beckers, "NOAO proposal to NSF for 8 m telescopes," Appendix N, Tech. Rep., NOAO (1989).
2. F. P. Wildi et al., "First light of the 6.5 m MMT adaptive optics system," *Proc. SPIE* **5169**, 17–25 (2003).
3. F. Quiros-Pacheco et al., "First light AO (FLAO) system for LBT: performance analysis and optimization," *Proc. SPIE* **7736**, 773609 (2010).
4. L. Baudouin et al., "Robust control of a bimorph mirror for adaptive optics," *Appl. Opt.* **47**(20), 3637–3645 (2008).
5. D. W. Miller and S. C. Grocott, "Robust control of the multiple mirror telescope adaptive secondary mirror," *Opt. Eng.* **38**(8), 1276–1287 (1999).
6. D. MacMynowski, R. Heimsten, and T. Andersen, "Distributed force control of deformable mirrors," *Eur. J. Control* **17**(3), 249–260 (2011).
7. R. Heimsten, D. MacMynowski, and T. Andersen, "Progress in developing a low-cost large deformable mirror," *Proc. SPIE* **7736**, 77365N(2010).
8. H. M. Martin et al., "Deformable secondary mirror for the LBT adaptive optics system," *Proc. SPIE* **6272**, 62720U (2006).
9. T. Andersen et al., "Novel concept for large deformable mirrors," *Opt. Eng.* **45**(7), 073001 (2006).
10. S. P. Timoshenko and S. Woinowsky-Krieger, *Theory of Plates and Shells*, 2nd Ed., McGraw-Hill International Edititions, New York (1959).
11. E. Ventsel and T. Krauthammer, *Thin Plates and Shells: Theory, Analysis, and Applications*, Marcel Dekker, New York (2001).
12. L. Meirovitch, *Analytic Methods in Vibrations*, The Mcmillan Company, New York (1967).
13. M. Abramowitz and I. Stegun, *Handbook of Mathematical Functions with Formulas, Graphs, and Mathematical Tables*, Dover Publications, New York (1965).
14. S. Hassani, *Mathematical Physics*, Springer-Verlag, New York (1999).
15. T. Ruppel, W. Osten, and O. Sawodny, "Model-based feedforward control of large deformable mirrors," *Eur. J. Control* **17**(3), 261–271 (2011).

Rikard Heimsten worked on constructing and testing a picosecond LIDAR system at the Combustion Physics department at Lund University, from 2004 until 2005. He graduated in 2005 at the Faculty of Engineering at Lund University with a MSc in engineering physics. Since 2006, he has been holding a PhD research position at the Institute in Astronomy and Theoretical Physics at the Lund University. His research interests include large deformable mirrors, control systems for adaptive optics, and integrated modeling.

Mette Owner-Petersen graduated in electrophysics engineering from the Technical University of Denmark (DTU) in 1967. In 1970 she received her PhD degree for the work "Cyclotron resonance in Si with special regard to quantum effects in the valence band" from the same university. From 1970 to 2000 she was a lecturer at the Physics Institute at DTU, teaching elementary-particle and nuclear physics, laser techniques, holography, and optics, and doing research in laser construction, Stark spectroscopy, and digital speckle interferometry. From 1991 to 1995 she worked for Nordic Telescope Group, concentrating on optical design of extremely large telescopes (ELTs) and instrumentation for the planned solar telescope LEST. Since 2000 she has held a position as lecturer at Lund Observatory, continuing her work with ELTs, and has participated in the European collaboration for a 50-m adaptive optics telescope, Euro50. The main area of her work is related to multiconjugate adaptive optics.

Thomas Ruppel worked on the Multi-Mirror-Telescope deformable mirror control systems as a DAAD scholar at the Optical Science Center in Tucson, Arizona, from 2006 until 2007. He received the DiplIng degree in Engineering Cybernetics from the University of Stuttgart, Germany in 2007. Since 2007, he has been holding a PhD research position at the Institute for System Dynamics at the University of Stuttgart, Germany. Currently, his main research interests include control of adaptive optics systems, control of distributed parameter systems, trajectory generation methods, and flatness-based control of linear and nonlinear systems.

Douglas MacMynowski is a Senior Research Associate in Control and Dynamical systems at the California Institute of Technology, where he has been involved in the design of the Thirty Meter Telescope since 2000. In addition to telescope control, his research interests span climate dynamics, flow control, and active noise control. Prior to joining Caltech, he was the Active Control Theme Leader at United Technologies Research Center. He received his PhD from M.I.T. in 1992.

Torben Andersen has a PhD in control engineering. From 1974 to 1979 he was in charge of the design of the Coudé Auxiliary Telescope at European Southern Observatory in Geneva. Subsequently he worked with steerable shipborne antennas for a few years. From 1984 to 1994 he was head of engineering for the Nordic Optical Telescope Scientific Association that built the Nordic Optical Telescope on La Palma and designed the 32-m EISCAT antenna on Spitsbergen. From 1994 to 1997 he was first head of systems engineering and later also head of telescope engineering for the VLT division of the European Southern Observatory. In 1997 he became a professor of optomechanical design at the Institute of Astronomy, Lund University, Sweden, and he is one of the architects behind Euro50, a proposed 50-m optical telescope with adaptive optics.

Downloaded from SPIE Digital Library on 11 May 2012 to 131.215.220.186. Terms of Use: http://spiedl.org/terms